N-((1-Benzyl-1*H*-1,2,3-triazol-4-yl)methyl)arylamide as a New Scaffold that Provides Rapid Access to Antimicrotubule Agents: Synthesis and Evaluation of Antiproliferative Activity Against Select Cancer Cell Lines

Jonathan A. Stefely,[†] Rahul Palchaudhuri,[‡] Patricia A. Miller,[†] Rebecca J. Peterson,[†]
Garrett C. Moraski,[†] Paul J. Hergenrother,[‡] and Marvin J. Miller*,[†]

[†]*Department of Chemistry and Biochemistry, University of Notre Dame, Notre Dame, Indiana 46556, and*
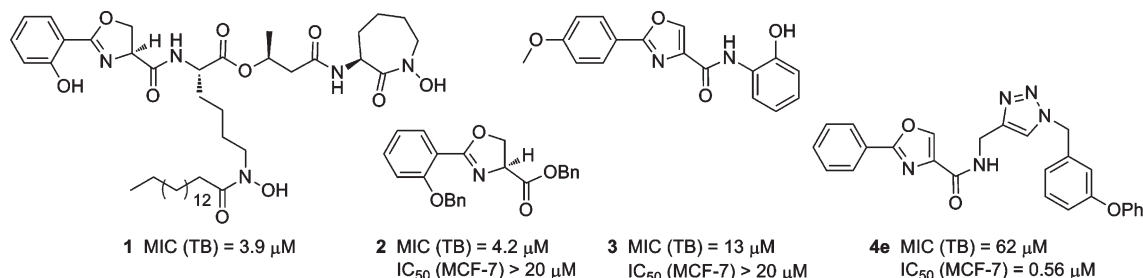[‡]*Department of Chemistry, Roger Adams Laboratory, University of Illinois, Urbana, Illinois 61801*

A series of *N*-((1-benzyl-1*H*-1,2,3-triazol-4-yl)methyl)arylamides was synthesized by copper-catalyzed azide−alkyne cycloaddition (CuAAC) and afforded inhibitors of cancer cell growth. For example, compound **13e** had an IC$_{50}$ of 46 nM against MCF-7 human breast tumor cells. Structure−activity relationship (SAR) studies demonstrated that (i) *meta*-phenoxy substitution of the *N*-1-benzyl group is important for antiproliferative activity and (ii) a variety of heterocyclic substitutions for the aryl group of the arylamide are tolerated. In silico COMPARE analysis of antiproliferative activity against the NCI-60 human tumor cell line panel revealed a correlation to clinically useful antimicrotubule agents such as paclitaxel and vincristine. This in silico correlation was supported by (i) in vitro inhibition of tubulin polymerization, (ii) G$_2$/M-phase arrest in HeLa cells as assessed by flow cytometry, and (iii) perturbation of normal microtubule activity in HeLa cells as observed by confocal microscopy. The results demonstrate that *N*-((1-benzyl-1*H*-1,2,3-triazol-4-yl)methyl)arylamide is a readily accessible small molecule scaffold for compounds that inhibit tubulin polymerization and tumor cell growth.

Introduction

Microtubules, dynamic protein polymers composed of α-tubulin and β-tubulin heterodimers, are a well-established cellular target for anticancer drugs.[1] Dynamic polymerization of tubulin is a necessary and tightly controlled process during mitosis.[2] Perturbing microtubule dynamics with small molecules blocks the cell cycle in the metaphase/anaphase transition and leads to apoptosis.[3] Thus, molecules[4] that target tubulin halt rapid cell division, a characteristic of cancer cells.[5] This therapeutic strategy has been validated by the clinical success of antimicrotubule drugs such as paclitaxel, docetaxel, vincristine, and vinblastine. Nonetheless, neurotoxicity and P-glycoprotein-mediated drug resistance limit the clinical utility of these drugs.[6] New-generation taxoids, vinca alkaloids, and other novel chemotypes that modulate microtubule dynamics have been synthesized in efforts to overcome these limitations.[7] For example, small molecule modulators of tubulin polymerization that do not elicit neurotoxicity in mice have been identified,[8] suggesting that neurotoxicity is not intrinsically linked to antimicrotubule agents. Nonetheless, few of these new antimicrotubule agents have produced useful clinical results. The key limitation to the development of new antimicrotubule drugs is a narrow therapeutic window.[9] A new antimicrotubule scaffold amenable to rapid derivatization and combinatorial library synthesis would provide an exceptional opportunity for the discovery of an efficacious antimicrotubule agent with an improved therapeutic window.

Herein we report the synthesis, in vitro antiproliferative activity against select cancer cell lines, and structure−activity relationships of compounds containing the *N*-((1-benzyl-1*H*-1,2,3-triazol-4-yl)methyl)arylamide scaffold. We also report mode of action studies based on in silico, in vitro, and cell culture experiments, which reveal the potent antimicrotubule activity of this scaffold. The discovery of this scaffold stemmed from our work on Mycobactin S (**1**),[10] a natural product produced by *Mycobacterium smegmatis* that exhibits antituberculosis activity[11] (Chart 1). All synthetic intermediates encountered during our group's total synthesis of Mycobactin S[12] were screened for biological activity. Surprisingly, benzyl ester **2**, a small fragment of the natural product, exhibited antituberculosis activity similar to that of Mycobactin S. Furthermore, in contrast to Mycobactin S, compound **2** provided a scaffold that was amenable to rapid structure−activity relationship studies, which led to the discovery of more potent antituberculosis agents.[13] While exploring derivatives of **2**, we found that 2-phenyl-oxazole-4-carboxamide derivative **3** was also active against *M. tuberculosis*. 2-Phenyl-oxazole-4-carboxamides are known inhibitors of histone deacetylase,[14] Stat3,[15] phosphodiesterase,[16] phosphatase,[17] thromboxane synthase,[18] kinase proteins,[19] and known activators of cellular caspase activity.[20] We synthesized derivatives of **3** to identify a more potent antituberculosis agent.[13] One of the derivatives, compound **4e**, had weak antituberculosis activity, but broader biological screening serendipitously revealed that **4e** and related derivatives have potent antimicrotubule activity in cancer cells, as disclosed in this report.

---

*To whom correspondence should be addressed. Phone: +1 574-631-7571. Fax: +1 574-631-6652. E-mail: mmiller1@nd.edu.

Chart 1. Structures of Antituberculosis Compounds **2** and **3** and Antimicrotubule Compound **4e**, All Derived from a Fragment of Mycobactin S (**1**)[a]

1 MIC (TB) = 3.9 μM

2 MIC (TB) = 4.2 μM
IC$_{50}$ (MCF-7) > 20 μM

3 MIC (TB) = 13 μM
IC$_{50}$ (MCF-7) > 20 μM

4e MIC (TB) = 62 μM
IC$_{50}$ (MCF-7) = 0.56 μM

[a] MIC values indicate in vitro antituberculosis activity against *M. tuberculosis* H37Rv in GAST medium,[21] and IC$_{50}$ values indicate in vitro antiproliferative activity against human breast cancer cell line MCF-7.

Scheme 1. Synthesis of 2-Phenyloxazole-4-carboxylic Acid
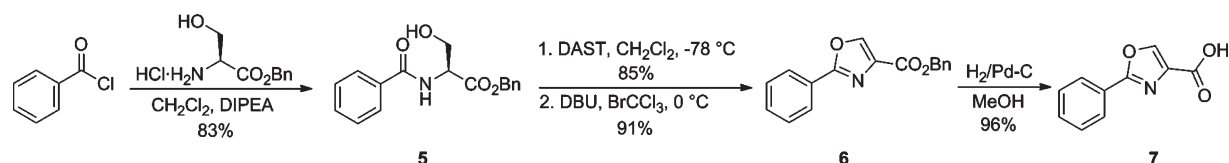
Scheme 2. Synthesis of *N*-((1-Benzyl-1*H*-1,2,3-triazol-4-yl)methyl)-2-phenyl-oxazole-4-carboxamide Scaffold

4a, R^1 = H
4b, R^1 = *p*-CH$_3$
4c, R^1 = *p*-CF$_3$
4d, R^1 = *m*-OCH$_3$
4e, R^1 = *m*-OPh
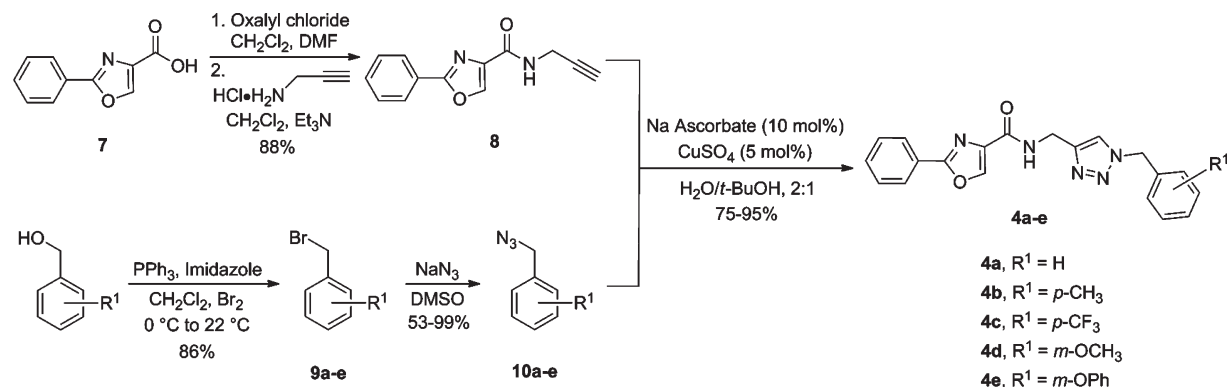
Results and Discussion

Chemistry. 2-Phenyl-oxazole-4-carboxylic acid **7** was synthesized according to the protocols shown in Scheme 1.[11,12] Coupling benzoyl chloride to serine benzyl ester hydrochloride afforded β-hydroxy amide **5**. Dehydrative cyclization and oxidation of β-hydroxy amide **5** with diethylaminosulfurtrifluoride (DAST) and DBU/BrCCl$_3$ yielded oxazole **6**.[22] Catalytic hydrogenolysis of the benzyl ester provided 2-phenyl-oxazole-4-carboxylic acid **7**.

Our strategy for exploring the chemical space around the 2-phenyl-oxazole-4-carboxamide fragment employed "click chemistry."[23] More specifically, we selected the Cu(I)-catalyzed azide–alkyne cycloaddition (CuAAC[a]) reaction[24] because of its wide scope, high efficiency, and recognized utility for drug discovery.[25] Following this strategy, *N*-((1-benzyl-1*H*-1,2,3-triazol-4-yl)methyl)-2-phenyl-oxazole-4-carboxamides **4a–e** were synthesized as shown in Scheme 2. Coupling propargylamine to freshly prepared 2-phenyloxazole-4-carboxyl chloride

(derived from the corresponding carboxylic acid **7**) provided alkyne **8**. With the terminal alkyne precursor in hand, we turned our attention to the syntheses of azides **10a–e**. Benzyl bromides **9a–e** were treated with NaN$_3$ to afford benzyl azides **10a–e**.[26] Exposing terminal alkyne **8** to benzyl azides **10a–e** in the presence of catalytic Cu(I) produced 1,4-disubstituted triazoles **4a–e** in high regioselectivity. Aqueous CuAAC conditions (H$_2$O/*t*-BuOH, 2:1) facilitated precipitation of the products, which were isolated with high purity.[24]

To explore the structure–activity relationships of the aryl amide group, a more general *N*-((1-benzyl-1*H*-1,2,3-triazol-4-yl)methyl)arylamide scaffold was synthesized according to the protocols shown in Scheme 3. The simplicity of reaction Schemes 2 and 3 is anticipated to allow the synthesis of a large library of 1,2,3-triazole-based structures. Moreover, the CuAAC reaction is the convergent synthetic step. Both the arylamide and benzyl groups, attached to opposite sides of the central triazole, are important components of the pharmacophore, as shown by the structure–activity studies described below. The convergence of the synthesis will allow both sides of the scaffold to be systematically varied in future SAR studies.

In Vitro Antiproliferative Activity. The antiproliferative activity of compounds **4a–e** against cancer cells was

[a] Abbreviations: CuAAC, copper-catalyzed azide–alkyne cycloaddition; MIC, minimum inhibition concentration to kill 90% of the bacterium; GI$_{50}$, 50% growth inhibition; TGI, total growth inhibition; LC$_{50}$, 50% lethal concentration, IC$_{50}$, half-maximal inhibitory concentration; TB, *Mycobacterium tuberculosis*; GAST, medium of glycerol-alanine-salts-Tween 80 without added iron; DBU, 1,8-Diazabicyclo-[5.4.0]undec-7-ene; SEM, standard error of the mean.

Scheme 3. Synthesis of *N*-((1-Benzyl-1*H*-1,2,3-triazol-4-yl)methyl)arylamide Scaffold
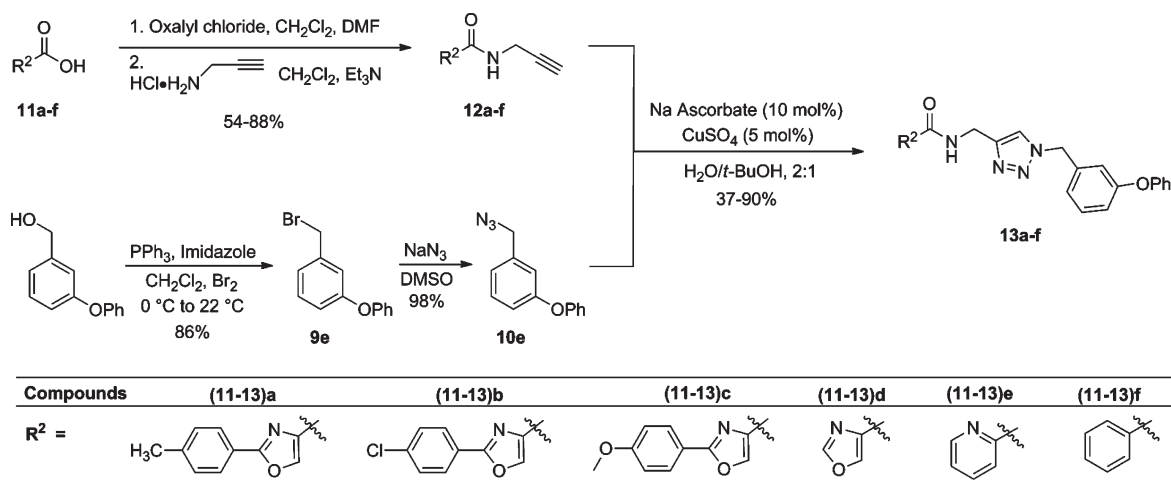
Table 1. In Vitro Antiproliferative Activity of Compounds **4a−e**, Colchicine, and 2-Methoxyestradiol against Human Breast Cancer Cell Line MCF-7

compd	R^1	IC$_{50}$ (μM) MCF-7
4a	H	15.9
4b	*p*-CH$_3$	7.59
4c	*p*-CF$_3$	7.33
4d	*m*-OCH$_3$	8.35
4e	*m*-OPh	0.56
	colchicine	0.013
	2-methoxyestradiol	0.84

Table 2. Antiproliferative Activities (IC$_{50}$) of Compounds **4e**, **13a−f**, **14**, Colchicine, and 2-Methoxyestradiol against Human Breast Cancer Cell Line MCF-7 and Human Lymphoma Cell Line U937

Compound	R^2	IC$_{50}$ (μM)[a] MCF-7	U937
4e		0.56 ± 0.11	1.40 ± 0.18
13a		0.33 ± 0.05	1.13 ± 0.44
13b		1.9 ± 1.4	nd
13c		0.66 ± 0.31	3.75 ± 1.78
13d		0.64 ± 0.35	2.19 ± 0.58
13e		0.046 ± 0.022	0.58 ± 0.42
13f		0.245 ± 0.007	nd
14		6.4 ± 1.3	28 ± 19
Colchicine		0.0134	0.008 ± 0.003
2-methoxyestradiol		0.842 ± 0.090	2.91 ± 1.17

[a] IC$_{50}$ values represent the concentration at which the cell count was inhibited to 50% of that measured in the vehicle control. Error is SEM, $n \geq 3$.

discovered during broad biological screening of a series of compounds originally anticipated to have antituberculosis activity. Although compounds **4a−e** had negligible antituberculosis activity, they inhibited the proliferation of cancer cells in vitro. Therefore, we determined the antiproliferative activities (IC$_{50}$ values) of hit compounds **4a−e** against the breast tumor-derived cell line MCF-7 (Table 1). Because the IC$_{50}$ of **4e** (0.56 μM) was significantly lower than those of **4a−d** (IC$_{50}$ = 7.3−16 μM), we conserved *meta*-phenoxy benzyl substitution at triazole N-1 in the second series of analogues (Scheme 3).

The structure−activity relationships of the triazole C-4 substituent were investigated by changing the carboxamide group (Table 2). In this SAR study, antiproliferative activity was investigated with the MCF-7 cell line and human lymphoma cell line U937. Addition of electron withdrawing or electron donating groups to the *para*-position of the 2-phenyloxazole group (**13a−c**) had a significant effect on antiproliferative activity, revealing an avenue for future optimization. Before performing an extensive SAR study via substitution of the 2-phenyloxazole group, we wanted to know if the 2-phenyloxazole was necessary for antiproliferative activity. If simpler aryl groups could replace the 2-phenyloxazole, the three-step synthesis of the 2-phenyloxazole-4-carboxylic acids could be bypassed by using commercial aryl acids. Thus, we conducted a systematic truncation of the 2-phenyloxazole-4-carboxamide group

found in **4e**. Removing the 2-phenyl group (**13d**) did not significantly change the activity. Following this lead, which suggested that we could use simpler aryl groups, we synthesized 2-pyridyl derivative **13e**. Against the MCF-7 cell line, the IC$_{50}$ of **13e** (46 nM) was significantly lower than that of **4e** (560 nM). Likewise, a significant decrease in IC$_{50}$ was observed with the U937 cell line. Therefore, replacing the 2-phenyloxazole group with simpler aryl groups represents a significant opportunity to improve antiproliferative activity. Phenyl derivative **13f** had improved antiproliferative activity compared to **4e** but was less active than 2-pyridyl derivative **13e**.
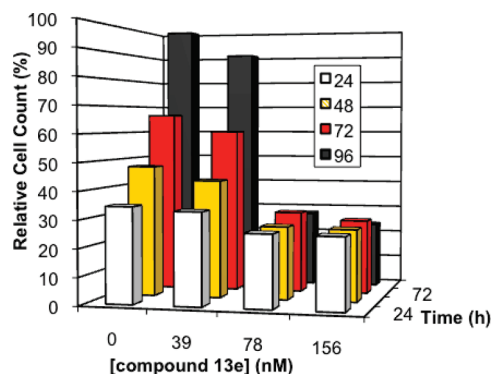
Figure 1. Time and concentration dependence of the antiproliferative activity of **13e** against MCF-7 tumor cells. Time is in terms of time elapsed after addition of the compound. Cell counts are shown relative to the cell count observed in the vehicle control 96 h after addition of the 0.5% DMSO solution.

Table 3. Antiproliferative Activity of Compounds **4b**, **4c**, **4d**, and **4e** against Selected Cell Lines in the NCI-60 Screen

compd	GI$_{50}$ (μM)			
	mean	HL-60	MCF-7	MDA-MB-435
4b	21.9	1.53	8.93	3.71
4c	16.6	2.34	3.83	1.94
4d	17.8	2.37	4.16	2.12
4e	0.87	0.39	0.36	0.18

Replacing the aryl group with a methyl group (**14**) gave a meaningful loss of antiproliferative activity and demonstrated the importance of the aryl carboxamide group.

Time Dependence of In Vitro Cellular Antiproliferative Activity. To distinguish cytotoxic activity from cytostatic activity, the time dependence of the effect of **13e** on MCF-7 cells was determined (Figure 1). At a concentration of 39 nM, **13e** slowed the cell proliferation rate. At higher concentrations (78 nM and 156 nM), cellular proliferation was halted, but **13e** did not decrease the number of cells. Thus, at concentrations moderately higher than the IC$_{50}$, **13e** is cytostatic rather than cytotoxic against MCF-7 cells.

Broad-Spectrum In Vitro Antiproliferative Activity. The NCI-60 anticancer drug screen is an in vitro assay consisting of 60 different human tumor cell lines.[27] Organized by disease type, the NCI-60 panel includes various leukemia cell lines and cell lines derived from solid tumor sources. Cell line selectivity guides further biological evaluation. In the NCI-60 panel, compounds **4b**, **4c**, **4d**, and **4e** induced broad-spectrum antiproliferative activity against tumor cell lines derived from leukemia, nonsmall cell lung cancer, colon cancer, CNS cancer, melanoma, ovarian cancer, renal cancer, prostate cancer, and breast cancer (see Supporting Information). Of these four compounds, **4e** (NCI-60 mean GI$_{50}$ = 870 nM) was more than 20 times more potent than the other three compounds (Table 3). This result is consistent with the results from our MCF-7 and U937 assays and further emphasizes the importance of *meta*-phenoxy benzyl substitution of triazole N-1 for optimal activity within this scaffold. With respect to selectivity among the 60 cell lines in the NCI-60 panel, all four compounds tested in the panel showed greater than average potency against human leukemia cell line HL-60, breast cancer cell line MCF-7, and melanoma[28] cell line MDA-MB-435 (Table 3).

COMPARE Analysis Revealed a Correlation to Antimicrotubule Drugs. For a given compound, the antiproliferative

Table 4. Matrix COMPARE Analysis of **4b**, **4c**, **4d**, and **4e**[a]

compd	**4b**	**4c**	**4d**	**4e**
4b	1.000	0.600	0.583	0.489
4c	0.600	1.000	0.968	0.475
4d	0.583	0.968	1.000	0.491
4e	0.489	0.475	0.491	1.000

[a] Matrix values (*r* values) are Pearson's correlation coefficients.[30]

Table 5. Standard COMPARE Analysis of **4e**[a]

rank	compd	*r*
	Based on GI$_{50}$ Mean Graph	
1	paclitaxel	0.541
2	maytansine	0.534
3	vincristine sulfate	0.500
4	trimetrexate	0.480
5	soluble Baker's Antifol	0.460
	Based on TGI Mean Graph	
1	paclitaxel (hiConc = 10^{-5} M)	0.654
2	paclitaxel (hiConc = 10^{-6} M)	0.646
3	paclitaxel (hiConc = $10^{-4.6}$ M)	0.642
4	maytansine	0.621
5	vinblastine sulfate	0.606
	Based on LG$_{50}$ Mean Graph	
1	rhizoxin (hiConc = 10^{-9} M)	0.681
2	rhizoxin (hiConc = 10^{-4} M)	0.650
3	vinblastine sulfate (hiConc = $10^{-7.6}$ M)	0.558
4	α-2'-deoxythioguanosine	0.545
5	vinblastine sulfate (hiConc = 10^{-4} M)	0.540

[a] The target set was the standard agent database and the target set end points were set equal to the seed end points (GI$_{50}$, TGI, and LC$_{50}$). Correlation values (*r*) are Pearson's correlation coefficients. Some hits appear multiple times because they were tested by the NCI for the Standard Agent Database at multiple concentration ranges.

activity measured in the NCI-60 differs by cell line. Furthermore, antitumor agents with similar mechanisms of action can produce similar patterns of differential antiproliferative data. We used the matrix COMPARE algorithm[29] to measure the correlations between compounds **4b**, **4c**, **4d**, and **4e** with respect to differential antiproliferative activity. The matrix produced by the analysis showed that **4c** and **4d** have highly correlated activities (*r* = 0.968) (Table 4). On the contrary, **4e** (the most potent compound tested in the NCI-60) had low correlations (*r* < 0.5) with the other three compounds. These matrix COMPARE results suggest that **4c** and **4d** have the same mechanism of action, but the mechanism of **4e** is distinct. Future studies will further investigate the importance of the *meta*-phenoxy substituent found in **4e** for its mechanism action. In the studies reported here, we focused on **4e** and related analogues, which also have the *meta*-phenoxy substituent, because of their superior potency.

The COMPARE algorithm can also compare the differential antiproliferative activity of a new compound to those of compounds with known mechanisms of action in the NCI Standard Agent Database.[31] Standard COMPARE analysis has been used previously to identify the cellular targets of antitumor agents.[32] Thus, the pattern of differential antiproliferative activity of **4e** was used to probe the NCI Standard Agent Database for correlations. We used all three measures of activity provided by the NCI-60 screen (GI$_{50}$, 50% growth inhibition; TGI, total growth inhibition; LC$_{50}$, 50% lethal concentration). A standard COMPARE analysis of **4e** (Table 5) showed correlations to paclitaxel, maytansine, vincristine, vinblastine, and rhizoxin, all of which affect

microtubule polymerization. Given this in silico result, we hypothesized that **4e** targets microtubules and directly tested
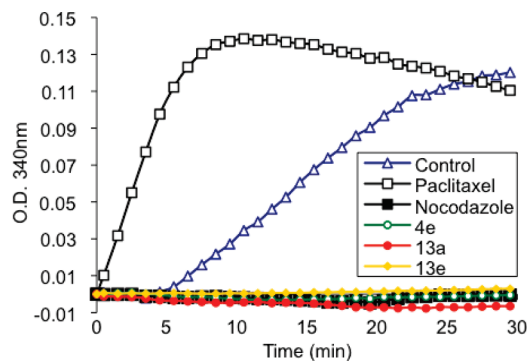

Figure 2. Inhibition of tubulin assembly by **4e**, **13a**, and **13e** in vitro. All compounds were tested at a concentration of 10 μM. Effects of compounds on tubulin polymerization were assessed by monitoring the increase in light scattering, measured as optical density (OD), at 340 nm. Standards of 10 μM nocodazole (a tubulin assembly inhibitor) and 10 μM paclitaxel (a tubulin assembly promoter) were used for direct comparison.
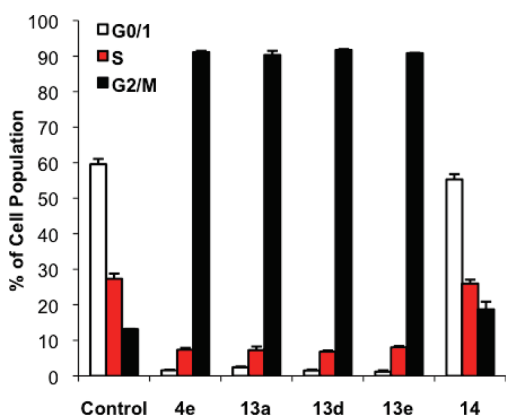
Figure 3. Effects of **4e**, **13a**, **13d**, **13e**, and **14** on the cell cycle distribution of HeLa cells as measured by propidium iodide staining and flow cytometry. HeLa cells were treated with 5 μM compound for 18 h in triplicate.

this hypothesis in vitro. In contrast, the first-ranked COMPARE hits for **4b−d** did not include antimicrotubule agents (see Supporting Information).

Inhibition of Tubulin Polymerization In Vitro. The polymerization of microtubules from purified tubulin can be monitored in vitro by measuring an increase in light scattering. This in vitro experiment removes complicating factors, such as microtubule-associated proteins (MAPs), which might be part of a putative target that leads to disruption of microtubules as observed with microscopy. To test our hypothesis that the target of the *N*-((1-benzyl-1*H*-1,2,3-triazol-4-yl)methyl)arylamide scaffold is tubulin, and not a MAP, we monitored the polymerization of tubulin after treatment with **4e**, **13a**, and **13e** (Figure 2). In this experiment, paclitaxel, a microtubule stabilizer, enhanced the rate of tubulin polymerization, while nocodazole, a microtubule destabilizer, prevented the polymerization of tubulin. Similar to nocodazole, **4e**, **13a**, and **13e** completely inhibited tubulin polymerization at 10 μM. Thus, the triazole-based compounds prevent the formation of microtubules in vitro. We followed this in vitro assay with cell culture experiments to see if microtubules are the primary cellular target.

Cell Cycle Analysis Demonstrated G$_2$/M-Phase Arrest. Antimicrotubule agents induce M-phase arrest. Flow cytometry can quantitatively determine the population of cells in each phase of the cell cycle by measuring the DNA content of individual cells. Cells in G$_2$-phase or M-phase have twice as much DNA as cells in G$_1$-phase. Thus, we conducted flow cytometric cell cycle analysis of HeLa cells treated with **4e**, **13a**, **13d**, **13e**, and **14**. Consistent with the hypothesized mechanism of action, compounds **4e**, **13a**, **13d**, and **13e** significantly increased the population of cells in G$_2$/M-phase (Figure 3). Upon treatment with these four compounds, the population of G$_2$/M-phase cells increased from 13% in the control to over 90%. Compound **14**, however, did not induce significant G$_2$/M-phase arrest, which suggested that the arylamide moiety is important for the antimitotic activity of the *N*-((1-benzyl-1*H*-1,2,3-triazol-4-yl)methyl)arylamide scaffold.

Confocal Microscopy Showed M-phase Arrest and Disruption of Microtubules. Visual evidence for M-phase arrest can
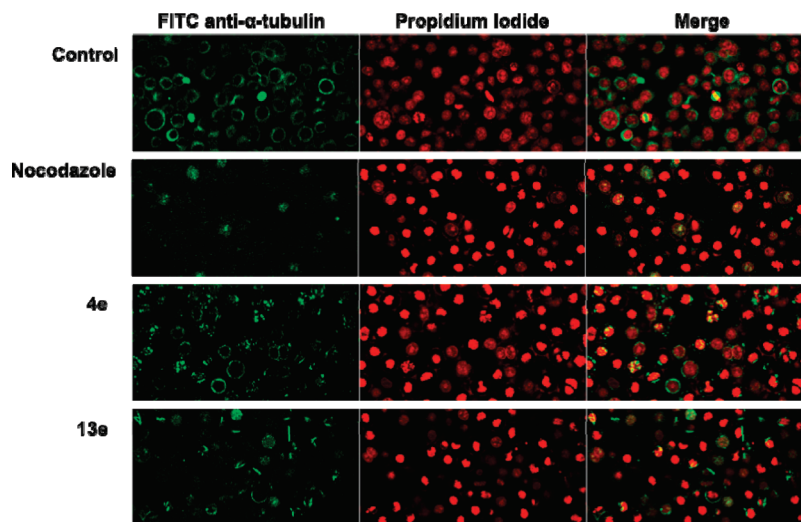

Figure 4. Confocal microscopy images of HeLa cells after 18 h incubation in the presence of 5 μM compound. Nocodazole is a known tubulin polymerization inhibitor. Nuclear DNA was stained with propidium iodide (red channel), and tubulin was stained with FITC-conjugated anti-α-tubulin antibody (green channel). Compounds **4e** and **13e** disrupted normal microtubule structures, caused fragmentation of mitotic spindles, and induced M-phase arrest.

be obtained with confocal microscopy due to DNA condensation, resulting in enhanced staining by propidium iodide. This outcome is in contrast to the diffuse staining of DNA in interphase cells. Visual evidence for the disruption of microtubules can be obtained concurrently using a fluorescein isothiocyanate-conjugated antitubulin antibody. We therefore used confocal microscopy to examine HeLa cancer cells treated with compounds **4e** and **13e**. Both DNA condensation and disruption of microtubules were observed at 5 μM of **4e** or **13e** (Figure 4). Together, these images show that **4e** and **13e** induce M-phase arrest and interfere with microtubule formation in whole cells.

Conclusion

In summary, we identified *N*-((1-benzyl-1*H*-1,2,3-triazol-4-yl)methyl)arylamide as a novel and proprietary[33] small molecule scaffold for potential antitumor agents. Elucidating structure–activity relationships by subtraction from initial hit compound **4e** (MCF-7 IC$_{50}$ = 560 nM) led to the discovery of **13e** (MCF-7 IC$_{50}$ = 46 nM), a foundational compound for further study. Compound **13e** (and related compounds) induced M-phase arrest in HeLa cells at 5 μM and inhibited tubulin polymerization in vitro at 10 μM, providing strong support for antimicrotubule activity as the primary mechanism of action. The NCI-60 screen demonstrated broad-spectrum antitumor activity and prompted further biological evaluation. Compound **13c** was recently evaluated by the National Cancer Institute Developmental Therapeutics Program (NCI DTP) for acute toxicity in vivo, and 100, 200, and 400 mg/kg intraperitoneal (IP) doses were well tolerated in nontumor-bearing mice. Ongoing studies in collaboration with the NCI DTP will evaluate in vivo efficacy in hollow fiber assays.[34] Extensive SAR studies and the development of a combinatorial library are accessible because compounds based on the *N*-((1-benzyl-1*H*-1,2,3-triazol-4-yl)methyl)arylamide scaffold are readily synthesized with the CuAAC reaction. Our findings will facilitate the design and optimization of potent, cell-permeable antimicrotubule agents.

Experimental Section

Purity of all samples are ≥95% as determined by HPLC or LC/HRMS.

2-(4-Methoxyphenyl)-*N*-((1-(3-phenoxybenzyl)-1*H*-1,2,3-triazol-4-yl)methyl)oxazole-4-carboxamide (C$_{27}$H$_{23}$N$_5$O$_4$, 13c). 2-(4-Methoxyphenyl)oxazole-4-carboxylic acid (**11c**, 0.951 g, 4.3 mmol) was suspended in anhydrous CH$_2$Cl$_2$ (12 mL) under argon. Oxalyl chloride (0.45 mL, 5.2 mmol) and *N*,*N*-dimethylformamide (20 μL) were added carefully to the mixture because of gas evolution. The reaction slowly turned to a light-yellow homogeneous solution over 3 h. The solution was concentrated in vacuo to give 2-(4-methoxyphenyl)oxazole-4-carbonyl chloride (1.0 g, 97%) as an yellow solid, which was used immediately in the next reaction without characterization.

2-(4-Methoxyphenyl)oxazole-4-carbonyl chloride (1.0 g, 4.0 mmol) was dissolved in anhydrous CH$_2$Cl$_2$ (15 mL) under argon and cooled to 0 °C (ice bath). Propargyl amine hydrochloride (0.443 g, 4.8 mmol) and *N*,*N*-diisopropylethylamine (2.1 mL, 12.0 mmol) were added with stirring. The reaction was allowed to warm to room temperature. After stirring for 20 h, TLC analysis indicated completion of the reaction. The mixture was poured into a solution of 10% aqueous NaHCO$_3$ and extracted with CH$_2$Cl$_2$ (2×). The organic layer was separated, washed with 10% aqueous NaHCO$_3$ and brine, dried with Na$_2$SO$_4$, filtered, and concentrated in vacuo. The resultant crude material was purified by column chromatography (SiO$_2$,

EtOAc/CH$_2$Cl$_2$ stepwise elution, 1:1 to 10:1) to give 2-(4-methoxyphenyl)-*N*-(prop-2-ynyl)oxazole-4-carboxamide (**12c**) as an off-white solid (0.788 g, 77%); mp 151−152 °C. ^{1}H NMR (300 MHz, CDCl$_3$) δ 8.06 (s, 1H), 7.82 (d, *J* = 8.5 Hz, 2H), 7.13 (bs, NH, 1H), 6.84 (d, *J* = 8.5 Hz, 2H), 4.15−4.07 (m, 2H), 3.72 (s, 3H), 2.15 (s, 1H). ^{13}C NMR (126 MHz, CDCl$_3$) δ 161.82, 161.57, 160.40, 140.49, 136.44, 128.83, 128.29, 119.13, 114.26, 113.69, 79.17, 71.69, 55.37, 28.66. HRMS−FAB (*m/z*) [M + H]$^+$ calcd for C$_{14}$H$_{12}$N$_2$O$_3$, 257.0921; found, 257.0930.

2-(4-Methoxyphenyl)-*N*-(prop-2-ynyl)oxazole-4-carboxamide (**12c**, 300 mg, 1.17 mmol) and 1-(azidomethyl)-3-phenoxybenzene (290 mg, 1.29 mmol) were suspended in a 2:1 mixture of water and *tert*-butyl alcohol (4.7 mL total volume). Sodium ascorbate (0.12 mmol, 0.12 mL, 1 M) and copper(II) sulfate (0.012 mmol, 0.12 mL, 0.1 M) were added sequentially. After stirring for 4 days at room temperature, TLC analysis indicated complete consumption of the reactants. The reaction mixture was diluted with water (5 mL) and cooled on ice. The white precipitate was isolated by vacuum filtration and washed with cold water (3 × 5 mL) and cold diethyl ether (3 × 3 mL) to afford 506 mg (90%) of pure product (**13c**) as a white powder. TLC R_f = 0.42 (EtOAc); HPLC t_r = 6.82 min (9:1 hexanes/2-propanol); mp 119.1−119.4 °C. ^{1}H NMR (300 MHz, CDCl$_3$) δ 8.18 (s, 1 H), 7.99−7.93 (m, 2 H), 7.60 (bs, NH, 1 H), 7.55 (s, 1 H), 7.39−7.28 (m, 3 H), 7.16−7.09 (m, 1 H), 7.03−6.90 (m, 7 H), 5.47 (s, 2 H), 4.72 (d, *J* = 6.1 Hz, 2 H), 3.88 (s, 3 H). ^{13}C NMR (151 MHz, CDCl$_3$) δ 161.83, 161.56, 160.84, 158.04, 156.36, 145.05, 140.26, 136.70, 136.29, 130.46, 129.85, 128.31, 123.79, 122.46, 122.27, 119.26, 119.18, 118.56, 118.04, 114.28, 55.40, 53.84, 34.46. HRMS−FAB (*m/z*) [M + H]$^+$ calcd for C$_{27}$H$_{23}$N$_5$O$_4$, 482.1823; found, 482.1803.

Supporting Information Available: Materials and methods, characterization data for all compounds, cell proliferation curves, cell cycle arrest profiles, and COMPARE analysis results. This material is available free of charge via the Internet at http://pubs.acs.org.

References

(1) Jordan, M. A.; Wilson, L. Microtubules as a Target for Anticancer Drugs. *Nat. Rev. Cancer* **2004**, *4*, 253–265.
(2) (a) Mitchison, T. J. Microtubule Dynamics and Kinetochore Function in Mitosis. *Annu. Rev. Cell Biol.* **1988**, *4*, 527–549. (b) Rusan, N. M.; Fagerstrom, C. J.; Yvon, A. C.; Wadsworth, P. Cell Cycle-Dependent Changes in Microtubule Dynamics in Living Cells Expressing Green Fluorescent Protein-α Tubulin. *Mol. Biol. Cell* **2001**, *12*, 971–980.
(3) Jordan, M. A. Mechanism of Action of Antitumor Drugs that Interact with Microtubules and Tubulin. *Curr. Med. Chem.: Anti-Cancer Agents* **2002**, *2*, 1–17.

(4) (a) Islam, M. N.; Iskander, M. N. Microtubulin Binding Sites as Target for Developing Anticancer Agents. *Mini-Rev. Med. Chem.* **2004**, *4*, 1077–1104. (b) Hadfield, J. A.; Ducki, S.; Hirst, N.; McGown, A. T. Tubulin and Microtubules as Targets for Anticancer Drugs. *Prog. Cell Cycle Res.* **2003**, *5*, 309–325. (c) Hamel, E. Antimitotic Natural Products and Their Interactions with Tubulin. *Med. Res. Rev.* **1996**, *16*, 207–231.

(5) Hanahan, D.; Weinberg, R. A. The Hallmarks of Cancer. *Cell* **2000**, *100*, 57–70.

(6) Kuppens, I. E. L. M. Current State of the Art of New Tubulin Inhibitors in the Clinic. *Curr. Clin. Pharmacol.* **2006**, *1*, 57–70.

(7) (a) Jordan, A.; Hadfield, J. A.; Lawrence, N. J.; McGown, A. T. Tubulin as a Target for Anticancer Drugs: Agents Which Interact with the Mitotic Spindle. *Med. Res. Rev.* **1998**, *18*, 259–296. (b) Kiselyov, A.; Balakin, K. V.; Tkachenko, S. E.; Savchuk, N.; Ivachtchenko, A. V. Recent Progress in Discovery and Development of Antimitotic Agents. *Anti-Cancer Agents Med. Chem.* **2007**, *7*, 189–208.

(8) Backer, G.; Beckers, T.; Emig, P.; Klenner, T.; Kutscher, B.; Nickel, B. New small-molecule tubulin inhibitors. *Pure Appl. Chem.* **2001**, *73*, 1459–1464.

(9) Wood, K. W.; Cornwell, W. D.; Jackson, J. R. Past and future of the mitotic spindle as an oncology target. *Curr. Opin. Pharmacol.* **2001**, *1*, 370–377.

(10) (a) Snow, G. A. Mycobactins: Iron-Chelating Growth Factors from Mycobacteria. *Bacteriol. Rev.* **1970**, *34*, 99–125. (b) White, A. J.; Snow, G. A. Isolation of Mycobactins form Various Mycobacteria: The Properties of Mycobactins S and H. *Biochem. J.* **1969**, *111*, 785–792.

(11) (a) Maurer, P. J.; Miller, M. J. Total Synthesis of a Mycobactin: Mycobactin S2. *J. Am. Chem. Soc.* **1983**, *105*, 240–245. (b) Hu, J.; Miller, M. J. Total Synthesis of a Mycobactin S, a Siderophore and Growth Promoter of Mycobacterium smegmatis, and Determination of its Growth Inhibitory Activity against Mycobacterium tuberculosis. *J. Am. Chem. Soc.* **1997**, *119*, 3462–3468.

(12) Vergne, A. F.; Walz, A. J.; Miller, M. J. Iron chelators from mycobacteria (1954−1999) and potential therapeutic applications. *Nat. Prod. Rep.* **2000**, *17*, 99–116.

(13) (a) Moraski, G. C.; Chang, M.; Villegas-Estrada, A.; Franzblau, S.; Möllmann, U.; Miller, M. J. Structure−Activity Relationship of New Antituberculosis Agents Derived from Oxazoline and Oxazole Benzyl Esters. *Eur. J. Med. Chem.* **2010**, *45*(5), 1703−1716. (b) Moraski, G. C.; Franzblau, S. G.; Miller, M. Utilization of the Suzuki Coupling to Enhance the Antituberculosis Activity of Aryl Oxazoles. *Heterocyles* **2010**, *80*, 977–988.

(14) Fennell, K. A.; Miller, M. J. Synthesis of Amamistatin Fragments and Determination of Their HDAC and Antitumor Activity. *Org. Lett.* **2007**, *9*, 1683–1685.

(15) Siddiquee, K. A. Z.; Gunning, P. T.; Glenn, M.; Katt, W. P.; Zhang, S.; Schroeck, C.; Sebti, S. M.; Jove, R.; Hamilton, A. D.; Turkson, J. An Oxazole-Based Small-Molecule Stat3 Inhibitor Modulates Stat3 Stability and Processing and Induces Antitumor Cell Effects. *ACS Chem. Biol.* **2007**, *2*, 787–798.

(16) Kuang, R.; Shue, H. J.; Blythin, D. J.; Shih, N. Y.; Gu, D.; Chen, X.; Schwerdt, J.; Lin, L.; Ting, P. C.; Zhu, X.; et al. Discovery of a highly potent series of oxazole-based phosphodiesterase 4 inhibitors. *Bioorg. Med. Chem. Lett.* **2007**, *17*, 5150–5154.

(17) (a) Rice, R. L.; Rusnak, J. M.; Yokokawa, F.; Yokokawa, S.; Messner, D. J.; Boynton, A. L.; Wipf, P.; Lazo, J. S. A Targeted Library of Small-Molecule, Tyrosine, and Dual-Specificity Phosphatase Inhibitors Derived from a Rational Core Design and Random Side Chain Variation. *Biochemistry* **1997**, *36*, 15965–15974. (b) Ducruet, A. P.; Rice, R. L.; Tamura, K.; Yokokawa, F.; Yokokawa, S.; Wipf, P.; Lazo, J. S. Identification of New Cdc25 Dual Specificity Phosphatase Inhibitors in a Targeted Small Molecule Array. *Bioorg. Med. Chem.* **2000**, *8*, 1451–1466.

(18) Takeuchi, K.; Kohn, T. J.; True, T. A.; Mais, D. E.; Wikel, J. H.; Utterback, B. G.; Wyss, V. L.; Jakubowski, J. A. Development of Dual-Acting Agents for Thromboxane Receptor Antagonism and Thromboxane Synthase Inhibition. 3. Synthesis and Biological Activities of Oxazolecarboxamide-Substituted ω-Phenyl-ω-(3-pyridyl)alkenoic Acid Derivatives and Related Compounds. *J. Med. Chem.* **1998**, *41*, 5362–5374.

(19) Morwick, T.; Berry, A.; Brickwood, J.; Cardozo, M.; Catron, K.; DeTuri, M.; Emeigh, J.; Homon, C.; Hrapchak, M.; Jacober, S. Evolution of the Thienopyridine Class of Inhibitors of IκB Kinase-β, Part I: Hit-to-Lead Strategies. *J. Med. Chem.* **2006**, *49*, 2898–2908.

(20) Tai, V. W. F.; Sperandio, D.; Shelton, E. J.; Litvak, J.; Pararajasingham, K.; Cebon, B.; Lohman, J.; Eksterowicz, J.; Kantak, S.; Sabbatini, P.; et al. Discovery and structure−activity relationship of 2-phenyl-oxazole-4-carboxamide derivatives as potent apoptosis inducers. *Bioorg. Med. Chem. Lett.* **2006**, *16*, 4554–4558.

(21) GAST medium is glycerol-alanine-salts-Tween 80 medium without added iron. See, (a) Voss, J. J. D.; Rutter, K.; Schroeder, B. G.; Su, H.; Zhu, Y.; Barry, C. E. The salicylate-derived mycobactin siderophores of *Mycobacterium tuberculosis* are essential for growth in macrophages. *Proc. Natl. Acad. Sci. U.S.A.* **2000**, *97*, 1252–1257. (b) Cho, S. H.; Warit, S.; Wan, B.; Hwang, C. H.; Pauli, G. F.; Franzblau, S. G. Low-Oxygen-Recovery Assay for High-Throughput Screening of Compounds against Nonreplicating Mycobacterium tuberculosis. *Antimicrob. Agents Chemother.* **2007**, *51*, 1380–1385.

(22) Phillips, A. J.; Uto, Y.; Wipf, P.; Reno, M. J.; Williams, D. R. Synthesis of Functionalized Oxazolines and Oxazoles with DAST and Deoxo-Fluor. *Org. Lett.* **2000**, *2*, 1165–1168.

(23) (a) Kolb, H. C.; Finn, M. G.; Sharpless, K. B. Click Chemistry: Diverse Chemical Function from a Few Good Reactions. *Angew. Chem., Int. Ed.* **2001**, *40*, 2004–2021. (b) Moses, J. E.; Moorhouse, A. D. The Growing Applications of Click Chemistry. *Chem. Soc. Rev.* **2007**, *36*, 1249–1262.

(24) (a) Rostovtsev, V. V.; Green, L. G.; Fokin, V. V.; Sharpless, K. B. A Stepwise Huisgen Cycloaddition Process: Copper(I)-Catalyzed Regioselective "Ligation" of Azides and Terminal Alkynes. *Angew. Chem., Int. Ed.* **2002**, *41*, 2596–2599. (b) Tornøe, C. W.; Christensen, C.; Meldal, M. Peptidotriazoles on Solid Phase: [1,2,3]-Triazoles by Regiospecific Copper(I)-Catalyzed 1,3-Dipolar Cycloadditions of Terminal Alkynes to Azides. *J. Org. Chem.* **2002**, *67*, 3057–3064.

(25) Kolb, H. C.; Sharpless, K. B. The Growing Impact of Click Chemistry on Drug Discovery. *Drug Discovery Today* **2003**, *8*, 1128–1137.

(26) Alvarez, S. G.; Alvarez, M. T. A Practical Procedure for the Synthesis of Alkyl Azides at Ambient Temperature in Dimethyl Sulfoxide in High Purity and Yield. *Synthesis* **1997**, *4*, 413–414.

(27) (a) Boyd, M. R.; Paull, K. D. Some Practical Considerations and Applications of the National Cancer Institute In Vitro Anticancer Drug Discovery Screen. *Drug Dev. Res.* **1995**, *34*, 91–109. (b) Shoemaker, R. H. The NCI60 Human Tumor Cell Line Anticancer Drug Screen. *Nature Rev. Cancer* **2006**, *6*, 813–823.

(28) (a) Ross, D. T.; Scherf, U.; Eisen, M. B.; Perou, C. M.; Rees, C.; Spellman, P.; Iyer, V.; Jeffrey, S. S.; Van de Rijn, M.; Waltham, M.; Pergamenschikov, A.; Lee, J. C. F.; Lashkari, D.; Shalon, D.; Myers, T. G.; Weinstein, J. N.; Botstein, D.; Brown, P. O. Systematic variation of gene expression patterns in human cancer cell lines. *Nat. Genet.* **2000**, *24*, 227–235. (b) Ellison, G.; Klinowska, T.; Westwood, R. F. R.; Docter, E.; French, T.; Fox, J. C. Further evidence to support the melanocytic origin of MDA-MB-435. *J. Clin. Pathol.: Mol. Pathol.* **2002**, *55*, 294–299.

(29) (a) Paull, K. D.; Shoemaker, R. H.; Hodes, L.; Monks, A.; Scudiero, D. A.; Rubinstein, L.; Plowman, J.; Boyd, M. R. Display and Analysis of Patterns of Differential Activity of Drugs Against Human Tumor Cell Lines: Development of Mean Graph and COMPARE Algorithm. *J. Natl. Cancer Inst.* **1989**, *81*, 1088–1092. (b) Zaharevitz, D. W.; Holbeck, S. L.; Bowerman, C.; Svetlik, P. A. COMPARE: a web accessible tool for investigating mechanisms of cell growth inhibition. *J. Mol. Graphics Modell.* **2002**, *20*, 297–303.

(30) (a) Paull, K. D.; Shoemaker, R. H.; Hodes, L.; Monks, A.; Scudiero, D. A.; Rubinstein, L.; Plowman, J.; Boyd, M. R. Display and Analysis of Patterns of Differential Activity of Drugs Against Human Tumor Cell Lines: Development of Mean Graph and COMPARE Algorithm. *J. Natl. Cancer Inst.* **1989**, *81*, 1088–1092. (b) Zaharevitz, D. W.; Holbeck, S. L.; Bowerman, C.; Svetlik, P. A. COMPARE: a web accessible tool for investigating mechanisms of cell growth inhibition. *J. Mol. Graphics Modell.* **2002**, *20*, 297–303.

(31) *DTP Human Tumor Cell Line Screen, Standard Agent Database*; Online: http://dtp.nci.nih.gov/docs/cancer/searches/standard_agent.html.

(32) (a) Bai, R.; Paull, K. D.; Herald, C. L.; Malspeis, L.; Pettit, G. R.; Hamel, E. Halichondrin, B; Homohalichondrin, B Marine Natural Products Binding in the Vinca Domain of Tubulin. *J. Biol. Chem.* **1991**, *266*, 15882–15889. (b) Paull, K. D.; Lin, C. M.; Malspeis, L.; Hamel, E. Identification of Novel Antimitotic Agents Acting at the Tubulin Level by Computer-Assisted Evaluation of Differential Cytotoxicity Data. *Cancer Res.* **1992**, *52*, 3892–3900. (c) Kuo, S. C.; Lee, H. Z.; Juang, J. P.; Lin, Y. T.; Wu, T. S.; Chang, J. J.; Lednicer, D.; Paull, K. D.; Lin, C. M.; Hamel, E.; Lee, K. H. Synthesis and Cytotoxicity of 1,6,7,8-Substituted 2-(4′-Substituted phenyl)-4-quinolones and Related Compounds: Identification as Antimitotic Agents Interacting with Tubulin. *J. Med. Chem.* **1993**, *36*, 1146–1156.

(33) Stefely, J. A.; Moraski, G. A.; Miller, M. J. Anti-cancer Compounds, Synthesis Thereof, And Methods Of Using Same. Patent WO/2009/111502, 2009.

(34) Hollingshead, M. G.; Alley, M. C.; Camalier, R. F.; Abbott, B. J.; Mayo, J. G.; Malspeis, L.; Grever, M. R. In vivo cultivation of tumor cells in hollow fibers. *Life Sci.* **1995**, *57*, 131–141.